Estuarine, Coastal and Shelf Science 206 (2018) 49–60

Contents lists available at ScienceDirect

Estuarine, Coastal and Shelf Science

journal homepage: www.elsevier.com/locate/ecss

A system shift in tidal choking due to the construction of Yangshan Harbour, Shanghai, China

Wenyun Guo [a, b], Xiao Hua Wang [a, b, c], Pingxing Ding [a, *], Jianzhong Ge [a], Dehai Song [c]

[a] State Key Laboratory of Estuarine and Coastal Research, East China Normal University, Shanghai 200062, China
[b] Sino-Australian Research Centre for Coastal Management, The University of New South Wales, Canberra, ACT 2610, Australia
[c] Key Laboratory of Physical Oceanography, Ministry of Education, at Ocean University of China, Qingdao 266100, China

ARTICLE INFO

Article history:
Received 15 May 2016
Received in revised form
4 January 2017
Accepted 8 March 2017
Available online 10 March 2017

Keywords:
Tidal choking
Tidal dynamics
Tidal energy
Land reclamation
Dredging
FVCOM

ABSTRACT

Tidal choking is a geometric feature caused by a narrowed channel. Construction of the Yangshan Harbour, Shanghai, China obstructed three key channels and intensively changed the local geometry and topography. In this study nine numerical experiments based on the Finite-Volume Community Ocean Model are conducted to study the project's influence on tidal characteristics. Results show that stronger tidal choking happened at the East Entrance after project, mainly due to the jet induced water-level drop forced by Bernoulli law and the longer and narrower geometry. The stronger tidal choking forces a faster flow and larger tidal energy flux at the choked channel while reducing the tidal amplitude in the Inner Harbour Area (IHA). The scouring on this channel reduces the choking effect but further enlarges tidal energy flux.

Moreover, damming the channels decrease the tidal amplitude at the lee side of tidal propagating direction while increasing the amplitude on the stoss side. The dams also decrease the tidal current on both sides, and meanwhile develop two patches with stronger current aside the dam. The project induced changes in tidal characteristics are complex in space, and perturbations in bathymetry increase this complexity. Yangshan Harbour's construction induces little changes in the total tidal energy density in the IHA, but induces obvious changes in the spatial distribution of tidal energy. Although this study is site-specific, the findings may be applicable to tidal dynamics in land reclamation close to open seas, such as the dramatic reclamation of islands in the South China Sea.

1. Introduction

Coastal zones and estuaries, as the transition between land and sea, are characterized by abundant natural resources; thus, there are large population and anthropogenic activities nearby. More and more coastal projects, such as reclamation and harbour constructions, are conducted for socio-economic development. These projects have significantly impacts on coastal environments and ecosystems. Understanding of these influences on tidal dynamics is benefit for project design in future and coastal management.

The most important physical setting in coastal waters is tides, the periodic sea level rising and falling caused by celestial motions. Tidal waves are strongly modified by friction, local geometry and rivers when they propagate into coastal zones and estuaries. Previous studies indicated that when tides travel into a narrow, frictional channel, their amplitudes are damped and phases are delayed (Keulegan, 1967; Kjerfve and Knoppers, 1991). This tidal choking phenomenon usually occurs in micro-tidal lagoons and bays with a shallow depth and narrow channel connecting to the open ocean (Kjerfve, 1986; Byun et al., 2004). The narrow channel acts like a hydraulic low-pass filter in a choked system, and dampens the amplitudes of high-frequency tides (Keulegan, 1967; Moody, 1988). Previous studies show that strong tidal choking occurs when a large-area tidal basin is connected to a large-amplitude open sea with long, narrow, shallow, and high-frictional channels (Hill, 1994; Byun et al., 2004).

Coastal constructions, particularly the projects with channels closed (open) can reinforce (weaken) the tidal choking. For example, the construction of dyke and two seawalls in the Mokpo Coastal Zone changed this region from a tidal-choked system to a

* Corresponding author.
E-mail addresses: guwin316319@gmail.com (W. Guo), X.Wang@adfa.edu.au (X.H. Wang), pxding@sklec.ecnu.edu.cn (P. Ding), jzge@sklec.ecnu.edu.cn (J. Ge), songdh@ouc.edu.cn (D. Song).

http://dx.doi.org/10.1016/j.ecss.2017.03.017
0272-7714/

non-choked one (Byun et al., 2004). Li et al. (2011) indicated that if the arms in Darwin Harbour were removed, tidal choking will disappear. Most of the tidal-choking studies focused on bays or tidal basins connecting oceans with one inlet (Keulegan, 1967; MacMahan et al., 2014). Few involved the tidal-choking effect in a multi-channel system, especially close to an open sea. The modification in tidal choking due to geometry change has also little been mentioned in previous studies.

Yangshan Deep-water Harbour (YDH) was constructed on an archipelago at the mouth of Hangzhou Bay (Fig. 1). This harbour's construction dammed three important channels and dramatically changed the geometry of this archipelago, which provides a perfect example to study tidal choking effect in a multi-channel system. The observed water-levels show that the constructions significantly altered the regional tidal characteristics, such as tidal amplitudes and phases, as well as the seabed siltation and erosion (SKLEC et al., 2006; Yang et al., 2012; Ying et al., 2011). We are therefore interested in examining the modification of tidal choking induced by the changes in geometry and bathymetry in a quantitative manner.

In this study, a numerical model based on the Finite-Volume Community Ocean Model (FVCOM) is adopted to study the changes in tidal choking and other tidal characteristics by the constructions. The physical mechanism of tidal choking is also explored. The study area, i.e., the Yangshan Harbour, Shanghai, China and the harbour's construction project are introduced in detail in Section 2. In Section 3, the Yangshan FVCOM nesting model is established and validated. Then Section 4 presents the FVCOM model results on changes in the predominant M_2 tide, tidal choking

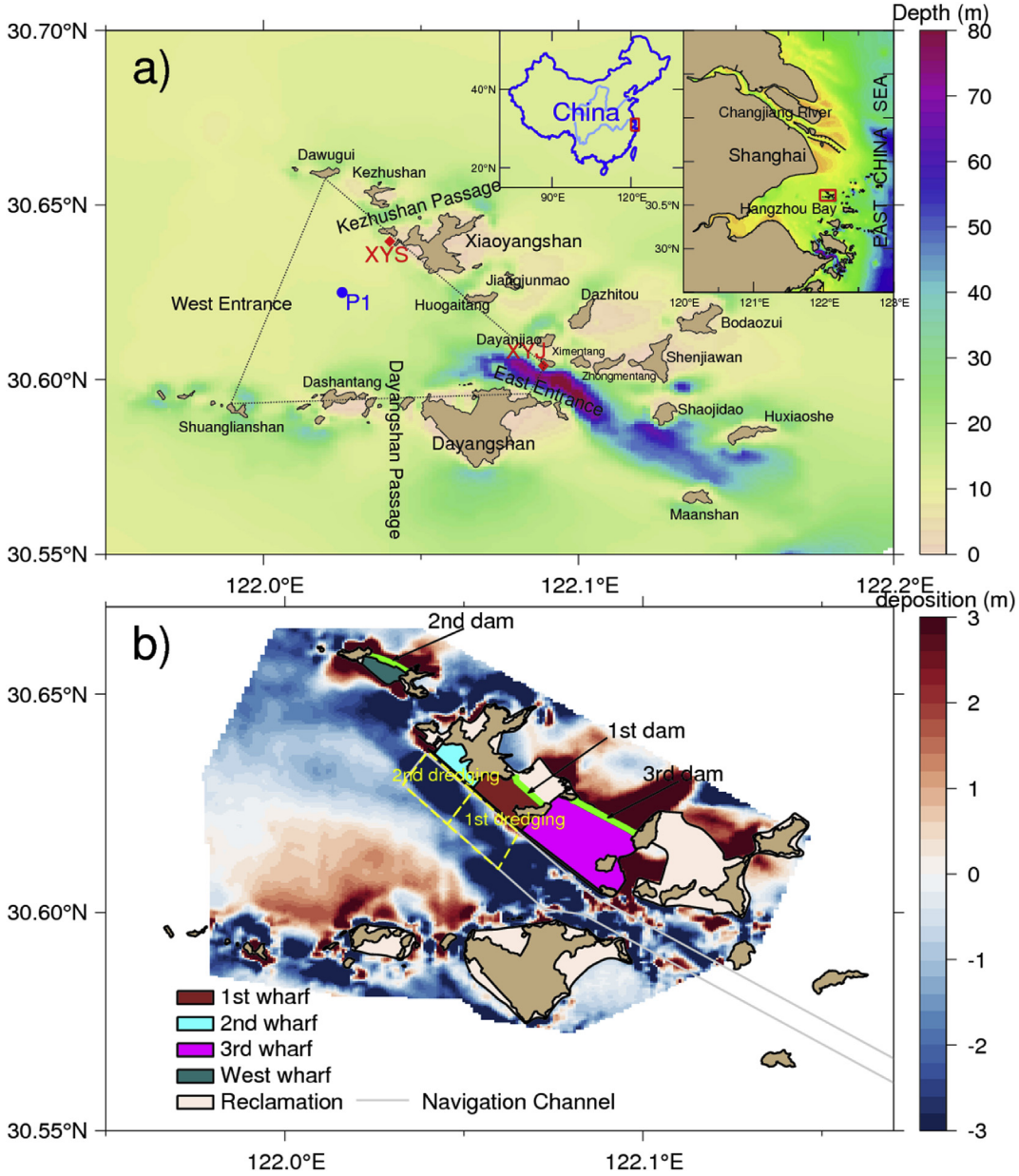

Fig. 1. (a) Location and bathymetry map of Qiqu Archipelago (Yangshan Harbour, in meters). Red diamonds mark the tidal elevation stations, blue dot marks the location of ADCP observation, dot-dashed polygon indicates the Inner Harbour Area (IHA). (b) The Yangshan project and the observed seabed change (in meters) from 1998 to 2008 around Yangshan Harbour. Yellow dashed boxes indicate the dredging areas, and green lines represent the dams. Timeline of this project is displayed at Table 1. (For interpretation of the references to colour in this figure legend, the reader is referred to the web version of this article.)

and tidal energy budget due to the construction project. Physical mechanisms for the change of tidal choking are explored in Section 5. Section 6 concludes this paper.

2. Study area

Yangshan Deep-water Harbour (YDH) was constructed as an extension of Shanghai Port in the Qiqu Archipelago, which is located at the junction of the Changjiang Estuary and Hangzhou Bay with ~32 km to the southeast of Shanghai (Fig. 1). The Qiqu Archipelago is characterized by complicated coastlines with 69 islands, indicating multiple channels. The islands form two chains, where Xiaoyangshan (XYS) Island belongs to the northern-island chain, and Dayangshan Island belongs to the southern-island chain. Between the two island chains, it has a wide (~8 km) and shallow (averaged depth of ~10 m) West Entrance, and a narrow (~1 km) but much deeper (maximum depth exceeding 85 m) East Entrance. Thus, the Inner Harbour Area (IHA, illustrated by the dash polygon in Fig. 1a), referring the area embraced by East Entrance, West Entrance and the two island chains, shelters the waves from open sea, where the annual-averaged wave height is only 0.47 m. Therefore, the hydrodynamics in the IHA is dominated by tides. And the maximum tidal range in the IHA can reach ~4.7 m. Tides propagate into the IHA through the East Entrance and other channels, and then move out from the West Entrance.

The construction of YDH started in 2002, and completed in 2008 (Fig. 1b), which had three phases with at least one channel closed at each phase. Detailed project progress is listed in Table 1. To satisfy the harbour's land demand, reclamation occurred in each phase. The harbour came into service in October 2005 when the dredging of first harbour basin was finished. During summer of 2006, the second harbour basin was also dredged to 16 m. Regular dredging followed to keep the navigation depth at 16 m, though the amount of dredging was very small. This engineering effort only kept one channel (Kezhushan Passage, Fig. 1b) open for the north-island chain, and thus greatly simplified the coastlines of the north-island chain. After the project, the East Entrance is significantly lengthened from 2 km to 4 km. Observed topography indicates that, after building each dam, two large sedimentation bands are formed immediately at both sides of the dam (Ying et al., 2011; Ying, 2012). Fig. 1b shows that obvious scouring happened in the channels. Details on observed topography change by the project can be found in Ying et al. (2011).

The extensive changes of coastlines and topography during the harbour's construction had strong impacts on the tidal characteristics (SKLEC et al., 2006; Yu, 2008; Yang et al., 2012). After the project was completed, the water-level difference between the East Entrance and Station XYS was enlarged dramatically (SKLEC et al., 2006; Wan, 2008). The harbour's construction changed flood-dominant current to a flood-ebb equilibrium according to the observations before 2007 (Wan, 2008). Analysis of the Sea-levels at Station XYS (Fig. 1a) showed that amplitudes of fourth-diurnal tides increased obviously after the project was completed (Yang et al., 2012; Yu et al., 2013). Other studies indicated that a circulation developed during high-water after the project was finished, which is regarded important to the sediment trapping (Li, 2009; Yang et al., 2012).

Table 1
Timeline of Yangshan Harbour construction projects.

Project	Time
1st Dam	4/2002~6/2003
2nd Dam	3/2003~5/2004
3rd Dam	5/2004~4/2005
1st Wharf	10/2002~6/2004
2nd Wharf	5/2004~10/2005
3rd Wharf	5/2005~12/2007
1st Dredging (16 m)	5/2005~10/2005
2nd Dredging (16 m)	5/2006~10/2006

3. FVCOM model description

3.1. FVCOM model setup

A high-resolution barotropic Yangshan FVCOM model is established to reproduce the tidal processes in the Yangshan Harbour sea area (Fig. 2). The Yangshan FVCOM model is nested in a well-validated larger-scale FVCOM model from Ge et al. (2013), which embraces the Changjiang Estuary and the Hangzhou Bay (Fig. 2a). The Yangshan FVCOM model covers all islands in the Qiqu Archipelago. The mesh grid considers the new boundaries after each project phase (Fig. 2c); so for different phases, it just needs to modify those cells with engineering works, without altering the others. This scheme can eliminate the imparity in simulated physical processes from mesh discrepancy, and is convenient to investigate the harbour's effects on local environment. The high-resolution mesh grid is up to 50 m along the new coastlines by the project and in the deep channels (Fig. 2c), providing accurate geometric fitting for the irregular coastlines and steep seabed.

The model is forced by four diurnal tides (K_1, O_1, P_1, Q_1), four semi-diurnal tides (M_2, S_2, N_2, K_2) and two quarter-diurnal tides (M_4, MS_4) with their amplitudes and phases specified at the open boundaries. The open boundary data are derived from an integrated East China Sea–Changjiang Estuary model (Ge et al., 2013). According to the observations by Wang et al. (2007), abundant Changjiang runoffs are mainly in a southward dispersion during May leaving less fresh water reaching YDH. Combining the strong tide-induced turbulent mixing, the water column is vertically well

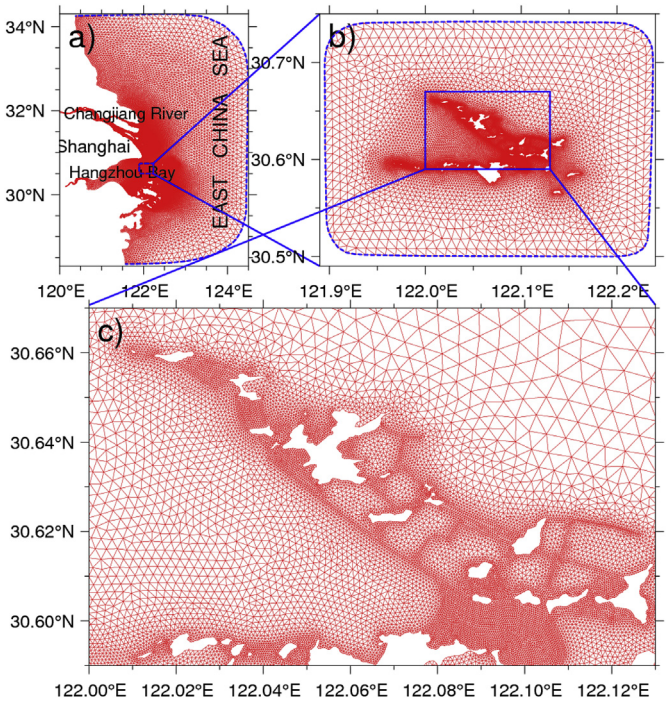

Fig. 2. Model mesh of (a) large-scale FVCOM model and (b) Yangshan FVCOM model. (c) Enlarged view of Yangshan FVCOM model mesh at the north-island chain. Spatial resolution of the mesh is high up to 50 m along all the project boundaries.

mixed in terms of both temperature and salinity. Additionally, the annual-averaged wind speed is less than 5.8 m s^{-1} in this study area, and the averaged wave height during May is less than 0.35 m. So, rivers, winds, waves, and other physical forcing factors are not considered in this modelling study, because they only have small influences on the sea-surface elevation in this area. Thus, the model is run in a barotropic condition. A wet/dry scheme (Chen et al., 2006, 2013) is included in the model using a critical depth of 0.05 m to deal with tidal flats.

3.2. FVCOM numerical experiments

To explore the changes in tidal choking due to the Yangshan Harbour project, nine numerical experiments, divided into two groups, for different construction periods and a control run (CR) are conducted (Table 2). Since a new phase had already started before the previous phase was finished (Table 1), it is difficult to find a time point to separate different project phases. Considering the mesh grid cannot be changed during the model integration, only the model setting that is the closest to the actual situation can be adopted. These experiments are mainly designed based on the closures of dams. Exp CR is the base case in 2001, before the project started. In Group A, the experiments are run at different engineering phases with bathymetric change considered. In Group B, the bathymetries are kept the same as that in CR. The bathymetric datasets were from the China Communications Construction Company Third Harbour Consultants Co., Ltd. Before 2004, there was only one bathymetric dataset for the study area, which was measured in 1998; so, it was used to approximate the topography before the project. Considering the slight accretion rate (~2.3 cm/a) of this sea area (Chen, 2000), this approximation is considered reasonable. The number in each experiment name represents the year (*e.g.*, Exp A8 represents the simulation for the year of 2008). All experiments are run for 40 days, including a spin-up of 5 days. The bathymetries for the nine experiments are derived from the observations taken closest to the simulation time.

3.3. FVCOM model validation

Station XYS is the only tidal station located at Yangshan Harbour and has measured sea-level data prior to the harbour's construction (Fig. 1a). Its hourly sea-level data in every fifth month of the year from 2001 to 2005 and in 2008 were gathered for this study. Moreover, during May 2008, there was a temporary sea-level station located at Xiaoyanjiao (shown as XYJ in Fig. 1a). The hourly-measured data at this station from 6 to 21 May were also collected. They are used to compare with the simulated water levels derived from Exps CR, A3, A4, A5, and A8. Results show that the model can reproduce the tidal elevation correctly. Fig. 3a displays the water-level comparison at XYS and XYJ in Exp A8. The absolute deviations at XYS in the five experiments are all less than 0.1 m, which is very small compared to the averaged tidal range of over 2.7 m. The model skill score (SS) (Allen et al., 2007) is applied to evaluate the simulated elevation:

$$SS = 1 - \frac{\sum_{i=1}^{N} (X_{\mathrm{mod}} - X_{obs})^2}{\sum_{i=1}^{N} (X_{obs} - \overline{X}_{obs})^2}, \quad (1)$$

where X is the variable of interest and $\overline{X}$ is the time mean. Performance levels are categorized as follows: >0.65 (excellent); 0.65–0.5 (very good); 0.5–0.2 (good); <0.2 (poor) (Allen et al., 2007; Ralston et al., 2010). SSs of the five experiments are all larger than 0.95, which indicates excellent tidal elevation simulations.

The harmonic amplitudes and phases at Station XYS derived from T_TIDE (Pawlowicz et al., 2002) are used to validate the tidal model (Table 3). The model gives a good assessment of amplitudes and phases of the astronomical tides K_1, O_1, M_2, and S_2 during different project phases, although S_2 phase is slightly underestimated (over 10°). The vectorial difference suggested by Foreman et al. (1993) is also to evaluate the model results:

$$Diff = \sqrt{(a_o \cos g_o - a_m \cos g_m)^2 + (a_o \sin g_o - a_m \sin g_m)^2}, \quad (2)$$

where (a_o, g_o) are the observed harmonic amplitude and phase, respectively; and (a_m, g_m) are the simulated ones. The results of *Diff* are presented in Table 3. In this region, M_2 is the strongest constituent followed by S_2. All *Diff* values are less than 0.15 m. The mean *Diff* of M_2 and S_2 are the same, which is 0.13 m. Overall, under the condition that the accurate geometry during the construction is hard to retrieve, and the observed bathymetries around Station XYS are sparse due to the shallow water, the differences of tidal constants between observations and our model outputs are reasonable, similar to those in many published studies (*e.g.*, Wu et al., 2011). This makes our results credible.

The model is also validated through a comparison of three-dimensional current structure. Successive 15-day Acoustic Doppler Current Profiler (ADCP) observations at Station P1 (see Fig. 1a for its location) were conducted during 5–21 May 2008. Current velocities were recorded hourly at six sigma levels. Comparison between observed and modelled tidal ellipses for the predominant M_2 tidal current is shown in Fig. 3b. The differences between observed semi-major axis and that of modelled are all less than 10%; the averaged difference of semi-minor axis is only 0.05 m s^{-1} and reaches its maximum (~0.1 m s^{-1}) in the bottom layer. There is a stable inclination deviation of about 10° at this station. It seems that the model tends to overestimate vertical mixing. Nevertheless, all errors are within a reasonable range, which indicates the credibility of this regional FVCOM model.

Table 2
Description of numerical experiments used in this study.

Exps	Depth	Project setting
CR	Nov, 1998	No
A3	Sep, 2003	1st dam and wharf
A4	May, 2004	Add 2nd dam on A3
A5	Apr, 2005	Add 3rd dam and 2nd wharf on A4
A8	Apr, 2008	All projects on
B3	Nov, 1998	Same with A3
B4	Nov, 1998	Same with A4
B5	Nov, 1998	Same with A5
B8	Nov, 1998	Same with A8

4. Model results and discussion

4.1. M_2 tide

According to the observed tidal constants at Station XYS (Table 3), the construction of the harbour has little effect on the amplitudes of diurnal tides K_1 and O_1 at this station, but caused a slight increase (~8 cm) on M_2 amplitude. Oscillations in S_2 amplitude is induced by this project. S_2 phase is delayed by 9° after the harbour's construction. The indistinctive changes in diurnal and semi-diurnal amplitudes result in an ambiguous trend of the form number F ($=(a_{O1} + a_{K1})/(a_{M2} + a_{S2})$) (National Ocean Service, 2000). As the indistinctive project influence on the S_2 and diurnal tides, we only focus on the prevailing M_2 tide.

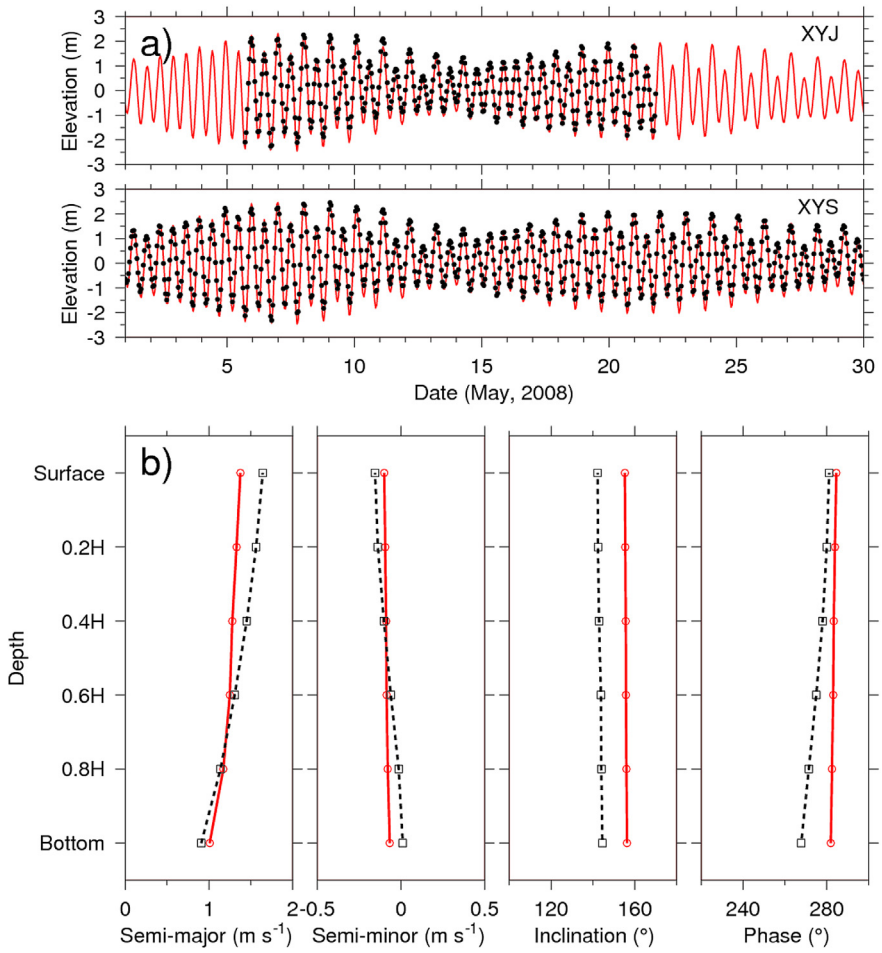

Fig. 3. Model-data comparison of (a) tidal elevation at Station Xiaoyanjiao (XYJ) and Xiaoyangshan (XYS); (b) M_2 current ellipse at Station P1. The red curves represent the FVCOM model output; the black dots in (a) and black dash lines in (b) signify the observed data. Station locations are given in Fig. 1a. (For interpretation of the references to colour in this figure legend, the reader is referred to the web version of this article.)

Table 3
Comparison between the modelled and observed amplitude (a in m) and phase (g in deg) of the four major tidal constituents K_1, O_1, M_2, and S_2 at Station XYS [a, b], where $F = (a_{O1} + a_{K1})/(a_{M2} + a_{S2})$ is the form number.

Year	F	K_1 (a/g)			O_1 (a/g)			M_2 (a/g)			S_2 (a/g)		
		Obs	Model	Diff	Obs	Model	Diff	Obs	Model	Diff	Obs	Model	Diff
2001	0.27	0.29/202	0.32/200	0.02	0.18/152	0.18/154	0.01	1.25/319	1.24/324	0.11	0.49/5	0.57/351	0.15
2003	0.29	0.32/202	0.34/200	0.02	0.18/152	0.19/149	0.02	1.28/318	1.25/324	0.13	0.47/8	0.53/355	0.13
2004	0.27	0.31/202	0.34/199	0.03	0.18/153	0.19/147	0.02	1.31/317	1.25/324	0.15	0.50/9	0.52/357	0.11
2005	0.28	0.32/202	0.32/197	0.03	0.19/156	0.20/153	0.01	1.32/319	1.23/324	0.15	0.47/11	0.48/357	0.12
2008	0.27	0.32/201	0.34/199	0.03	0.18/158	0.19/151	0.03	1.33/320	1.26/324	0.11	0.49/14	0.51/358	0.14

[a] Obs: observed; Diff: the vectorial difference suggested by Foreman et al. (1993).
[b] Mean Diff of K_1 is 0.03 m; O_1 is 0.02 m; M_2 is 0.13 m; S_2 is 0.13 m.

Fig. 4a shows the modelled M_2 tidal constants before the construction of YDH (Exp CR). The M_2 tide propagates through YDH area from east to west, its amplitude increases gradually throughout the propagation accompanying perturbation from the islands. The islands Bodaozui, Shenjiawan and Shaojidao form a line to block the tidal propagation and decrease the M_2 amplitude at the lee. After tide propagates through the East Entrance, a slight drop of the M_2 amplitude also happens, showing a slight tidal choking effect. The islands also affect the tidal wave celerity, and thus complicate the M_2 phase lag.

After the construction of YDH, if the bathymetrical change is not considered (Fig. 4b), the M_2 amplitude is reduced by ~ 1 cm and phase is delayed by over 0.5° in the IHA; while on the north side of the north-island chain, the M_2 amplitude is amplified by ~1 cm, accompanying more advanced M_2 phase by over 0.5°. All these changes are confined in a radius of 4 km around the constructions. The most dramatic amplitude decrease (over 3 cm) happens in the narrow East Entrance.

The bathymetrical change makes the change pattern more complex (Fig. 4c). A small increase (~1 cm) of M_2 amplitude around the Kezhushan Passage developed after this project. Both the deeper topography in this channel and the dredging of the harbour basin (not shown), which started in 2005, can contribute to this increase. In the East Entrance, the deeper bathymetry reduces the

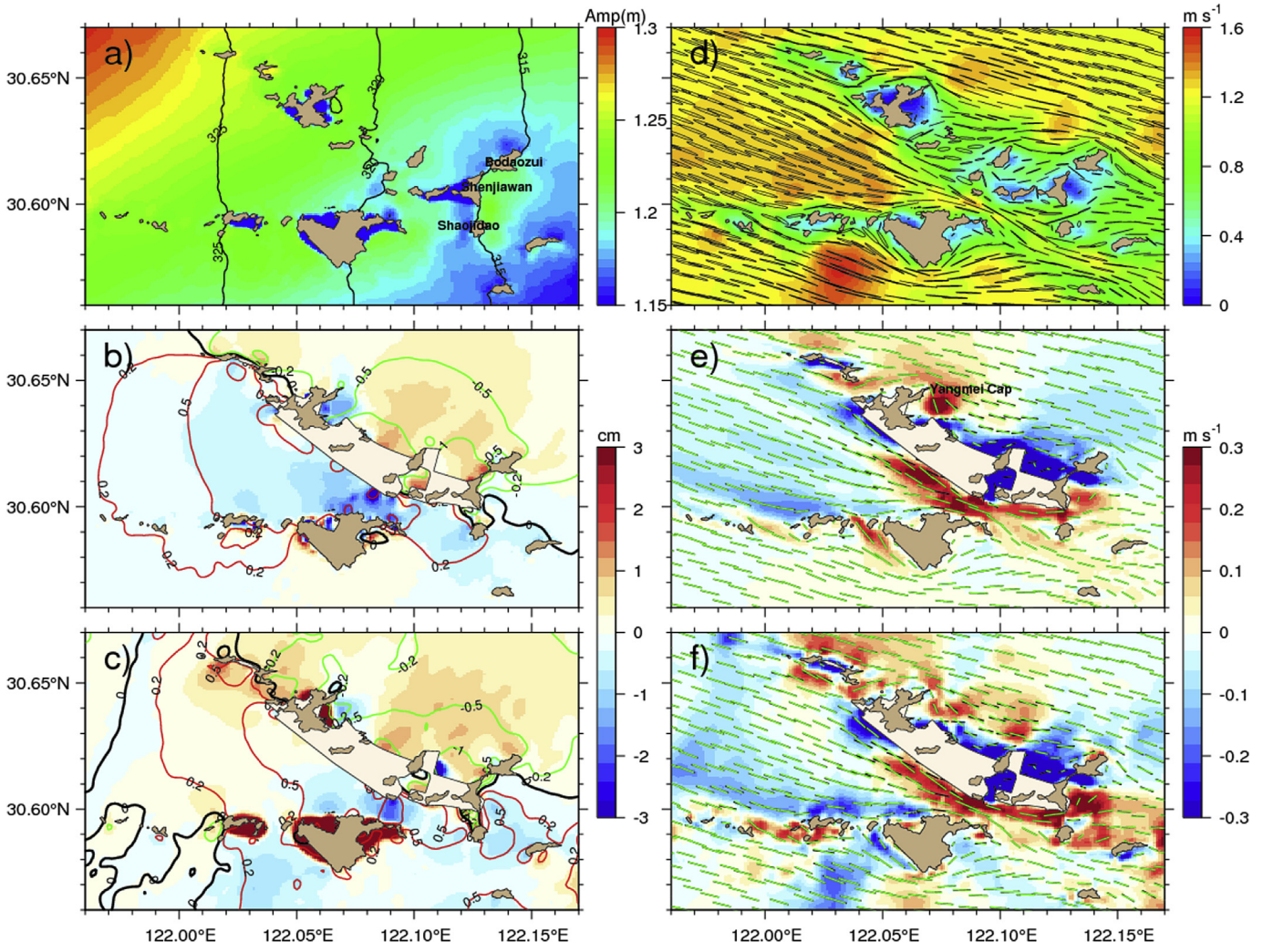

Fig. 4. (a) Colour scale shows the M_2 elevation amplitude (unit: m) and the M_2 co-phase lines are labelled in 5° step. (b) Colour scale shows the change of M_2 elevation amplitude (unit: cm) of Exp. B8 − CR. The red lines show the correspond contours of M_2 phase change of 0.2°, 0.5° and 1°, and the contours of phase change in −0.2°, −0.5° and −1° are shown in the green lines. (c) Same with (b) but for Exp. A8 − CR. (d) Distribution of the M_2 tidal ellipse of Exp CR. Colour scales show the magnitude of M_2 major axis (unit: m s^{-1}). (e) Colour scales show the difference of M2 major axis (unit: m s_{-1}) of Exp. B8 − CR. Black and green lines denote the direction of M_2 major-axis in Exp CR and Exp. B8, respectively. (f) Same with (e) but for Exp. A8 − CR. (For interpretation of the references to colour in this figure legend, the reader is referred to the web version of this article.)

decrease magnitude of M_2 tide. Comparison of Fig. 4b and c, we can conclude that the amplitude increase at Station XYS is mainly due to the siltation around it. The large increase in M_2 amplitude around Dayangshan island is due to the bathymetry changes resulting from the reclamation there. In overall, the influence of harbour's construction arises only in a small region around the construction sites, but the bathymetrical change would further enlarge the influenced area.

Fig. 4d displays the M_2 ellipse and the distribution of the major-axis of Exp CR before project. The M_2 ellipticity is small in the IHA (<0.1), thus the flow system can be treated as alternating current system. Around the islands, the M_2 current is small due to the shallow topography. While in the centre of the IHA and in the deep East Entrance, the M_2 current is strong. In addition, the mainstream is approximately along the east-west direction.

The harbour's construction enhances the M_2 tidal current in all the remaining tidal channels, except the West Entrance (Fig. 4e). In the harbour basins, the flow is regulated along the new straight coastline, resulting the M_2 current inclination in the third harbour basin more northward by ~10°. This leads to stronger current in the navigation channel (shown in Fig. 1a) and the weaker current in the south and centre IHA, thus formatting the bathymetrical change pattern summarized as 'scouring in north and siltation in south' (Ying et al., 2011; Yu et al., 2013), which is in favour of the maintenance of navigation depth (16 m). On the north side of the north-islands chain, most sea area behaves decreased M_2 current, but on the east of the Xiaoyangshan island, there is a small patch behaving stronger M_2 current, mainly forced by the Yangmei Cap of the Xiaoyangshan island.

The overall change pattern of M_2 tidal current has not be altered by the bathymetrical changes (Fig. 4f), but some disturbance occurs. In the Dayangshan Passage, the current is weakened, mainly due to the stronger island wake effect (Wolanski and Hamner, 1988; Furukawa and Wolanski, 1998). The stronger current route from the Shenjiawan-Shaojidao Channel through the East Entrance to the first harbour basin, which is induced by the harbour's construction, is enhanced by the overall deeper bathymetry in this route. In the IHA, the erosion in the north with the contribution of dredging, and siltation in the south force the current more northward and weaken the current in the south.

Detailed study shows that after the construction of each dam, M_2 amplitude is reduced in the lee, accompanying by delayed M_2

phase. Meanwhile, in the stoss side, the amplitude is amplified accompanying by advanced phase (Fig. 5a–c). The area of amplitude decrease in the lee caused by the second dam is much smaller than that caused by the first and third dam. The nearly

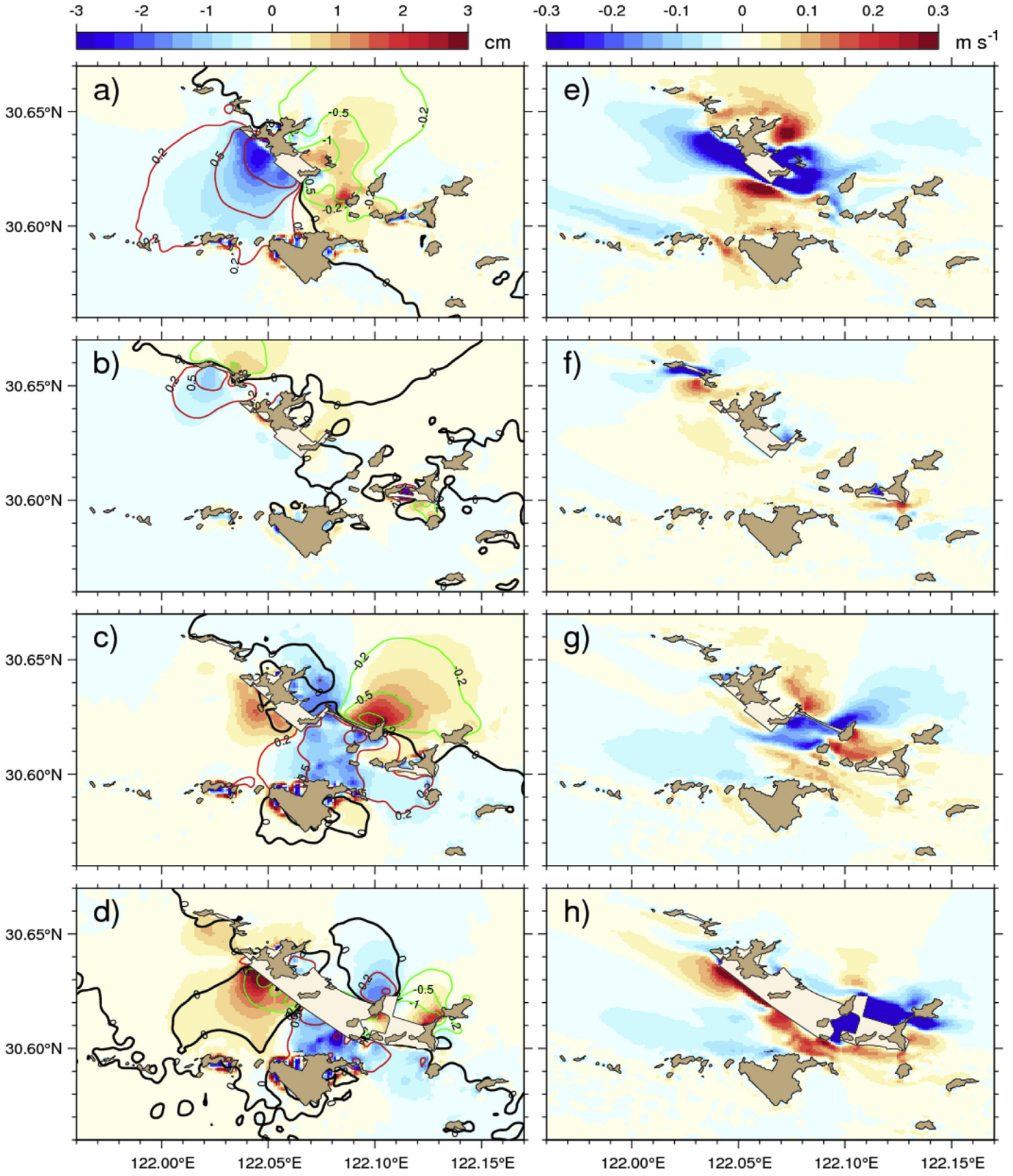

Fig. 5. Left column: Difference of M_2 amplitude (units: cm) of (a) Exp B3 − Exp CR, (b) Exp B4 − Exp B3, (c) Exp B5 − Exp B4, and (d) Exp B8 − Exp B5. Red lines show the correspond contours of M_2 phase change of 0.2°, 0.5° and 1°, and the contours of phase change in −0.2°, −0.5° and −1° are shown in the green lines. Right column: Difference of M_2 semi-major axis (unit: m s^{-1}) of (e) Exp B3 − Exp CR, (f) Exp B4 − Exp B3, (g) Exp B5 − Exp B4, and (h) Exp B8 − Exp B5. (For interpretation of the references to colour in this figure legend, the reader is referred to the web version of this article.)

parallel relation between the direction of the dam and the direction of tidal propagation may be the main factor for this. The bathymetrical changes superimpose some disturbances on this pattern, but not shift it (not shown). Obvious M_2 amplitude-decrease, implying stronger tidal choking, happens at the East Entrance by the construction of the third dam and third wharf (Fig. 5c and d).

The construction of each dam blocks the tidal current and cause two bands of weaker current at both sides of it (Fig. 5e–g). Simultaneously, there are two patches near the dam accompanying stronger M2 current. This change pattern is further strengthened by the bathymetric changes (not shown). The weaker current in the south of IHA is mainly induced by the construction of third dam (Fig. 5g), and enhanced by the third wharf (Fig. 5h), and the siltation there (not shown). The third dam also causes stronger current in the East Entrance, which is further enhanced by the third wharf.

4.2. Tidal energy budget

The channels in the YDH function as a network for water, sediment and tidal energy exchange between the IHA and the open seas. Assessment evolution of each channel's role in the tidal energy exchange along the construction of YDH is important to understand the tidal dynamics and the water circulation in the IHA (Fang et al., 1999; Zu et al., 2008; Chen et al., 2009; Song et al., 2013).

The total tidal energy density, including potential tidal energy and kinetic tidal energy, per unit area can be calculated as

$$E = \frac{1}{2}\rho\left(g\zeta^2 + D|\vec{v}|^2\right) \tag{3}$$

where ρ is the water density, g is the gravitational acceleration, ζ is the water surface elevation, $D = H + \zeta$, and H is the water depth, $\vec{v}$ is the velocity vector.

And tidal energy flux over a unit width within one tidal cycle can be estimated using

$$\vec{E}_f = \frac{1}{T}\int_0^T \rho D\left(g\zeta + \frac{1}{2}|\vec{v}|^2\right)\ \vec{v}\ dt \tag{4}$$

where T is the tidal period.

The tidal energy flux and tidal energy density of Exp. CR, B8 and A8 are displayed in Fig. 6, and statistics of the tidal energy flux in the channels are shown in Table 4. Integrating the tidal energy flux

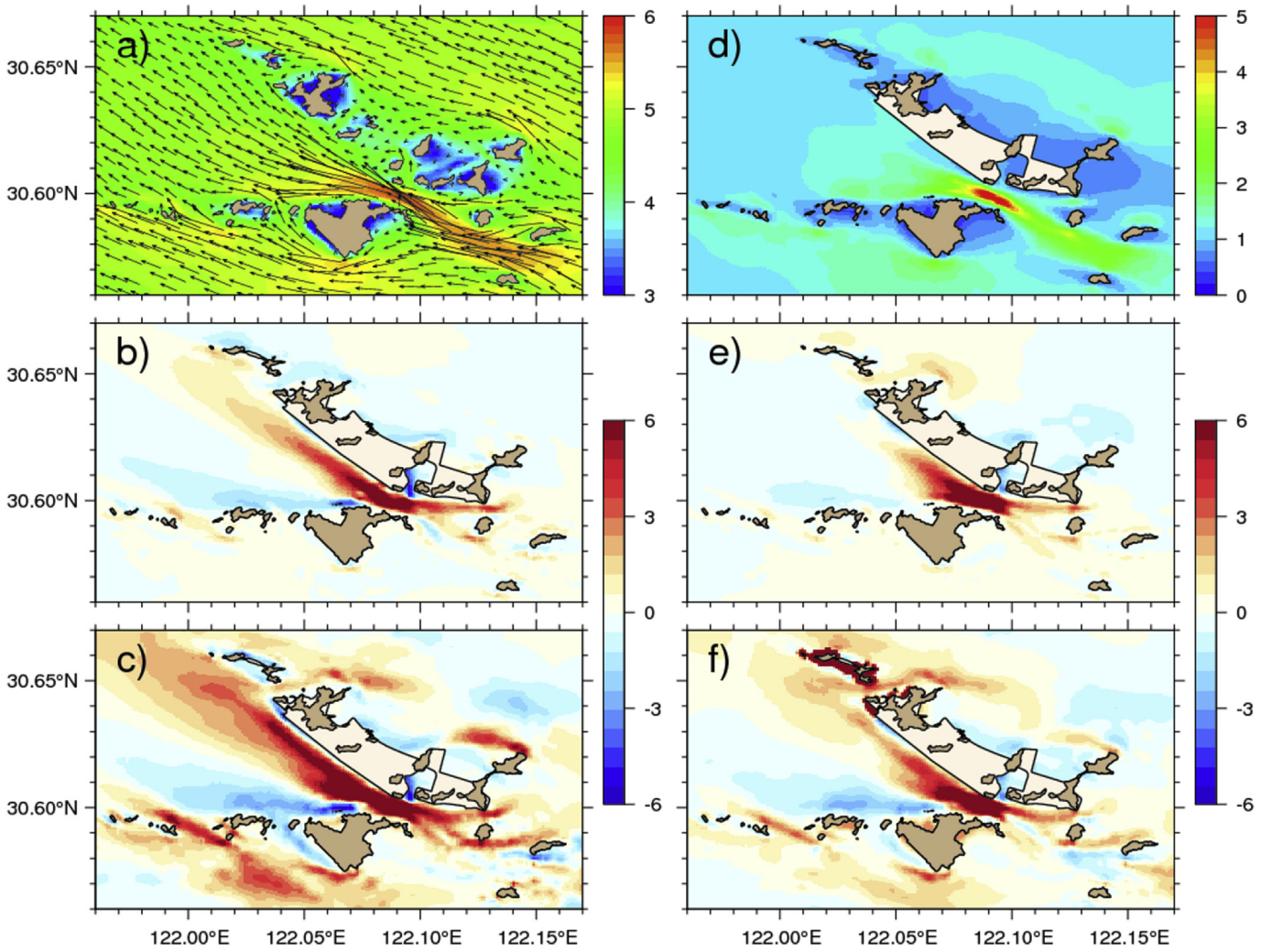

Fig. 6. (a) Tidal energy flux (unit: W m^{-1}, shown in logarithmic values base 10) in Exp. CR. (b) and (c) show the changes of tidal energy flux (unit: $\times 10^4$ W m^{-1}) of Exp B8 − CR and Exp A8 − CR, respectively. (d) Tidal Energy Density (unit: $\times 10^4$ W m^{-2}) of Exp. CR. (e) and (f) show the changes of tidal energy density (unit: $\times 10^3$ W m^{-2}) of Exp B8 − CR and Exp A8 − CR, respectively.

Table 4
Tidal Energy Budget of the Nine Numerical Experiments (unit: MW s^{-1}). Positive values indicate that tidal energy flux into the IHA.

	CR	B3	B4	B5	B8	A3	A4	A5	A8
East Entrance	35.3	35	35.1	37.2	40.6	34.9	38.4	38.7	43.6
Southern Channels	15.5	16.8	16.9	16.5	16.3	16.7	16.1	18	17.6
West Entrance	−52.5	−51.3	−52.3	−52.5	−53	−51.5	−55.9	−56.7	−59.4
Northern Channels	6.4	4.2	5.2	3.6	1.1	4.7	6.1	4.7	3
Dissipation	4.8	4.7	4.9	4.8	4.9	4.7	4.7	4.6	4.8
Total in	57.3	56	57.1	57.2	57.9	56.3	60.6	61.3	64.2

along the dash closed sections shown in Fig. 1a, the dissipation of tidal energy in the IHA is obtained. There are two main mechanisms dissipating tidal energy: bottom friction and horizontal viscosity. Before project, tidal energy of 57.8 MW is transported into the IHA per second, through the East Entrance (62%) and the channels in the Northern (11%) and Southern (27%) Island Chain. Over 90% of the tidal energy then delivers out through the West Entrance and the rest are dissipated in the IHA, mainly due to the bottom friction (~90%).

Since the limited tidal energy flux in the northern-island chain, constructions on it bring only some mild changes to the tidal energy budget. Comparing Exp. B8 and CR, it is found that the project results in more tidal energy flux by 9% in the East Entrance (Table 4). The harbour blocks the tidal energy from the northern channels, permitting the vast tidal energy coming from the East Entrance to keep their transport direction. This results in more tidal energy delivering through the north IHA but less through the south IHA (Fig. 6b). This feature is further enhanced by the scouring in the East Entrance and the scouring in the north IHA (including the dredging) (Fig. 6c).

Moreover, the stronger tidal energy flux in the East Entrance leads to the corresponding increase of the tidal energy density. As Fig. 5 shows, in the channels, the velocities are increased obviously but water elevation not. This lead to the area-mean kinetic tidal energy density in the IHA increased a little from 7.03 kW m^{-2} in Exp. CR to 7.41 kW m^{-2} in Exp. B8 and 7.59 kW m^{-2} in Exp. A8. The increase is mainly due to the construction of third wharf. While the area-mean potential tidal energy density changes little during the constructions. According to Table 4 and Fig. 6, we can conclude that the construction of YDH leads to little changes in the total tidal energy density in the IHA but obvious changes in the spatial distribution of tidal energy.

More details show that the construction of first dam lead to an obvious decrease of (~35%) tidal energy flux in the northern channels, but the second dam increases the tidal energy flux in the Kezhushan Passage, and then the third dam decrease the tidal energy flux in the northern channels by 30%. Comparing Exp. B8 and A8, scouring in the Kezhushan Passage leads to increase in tidal energy flux, showing the modulation of bathymetries affecting the tidal propagation. Similar effect also occurs in the East Entrance. But in the Dayangshan Passage, tidal energy flux is decreased by the scouring (comparing Fig. 6b and c), may due to the stronger island wake effect of Dayangshan island.

4.3. Physical mechanism for stronger tidal choking at the East Entrance

Dams in channels cause changes of tidal dynamics in remain channels, resulting in shifts of tidal choking effect. Considering the crucial function of the East Entrance for tidal energy transport in the YDH, the shift of tidal choking effect along with the constructions of the YDH is understood in the section. The tidal constants along a cross section as shown in Fig. 7a are analysed. The depth of the cross section had its maximum value of nearly 90 m at the East Entrance before the project (Fig. 7b). There was a small hill on the east of the East Entrance at 14 km of the cross section, about 20 m higher than the adjacent seabed. The seabed along this cross section has been eroded after the harbour's construction, especially at the deep East Entrance. Before the project, there was a small drop of M_2 amplitude at the East Entrance (see the bold grey line Fig. 7c), and reached the minimal value at distance of 11.2 km. A slightly more delayed M_2 phase also occurred at the East Entrance concomitantly (not shown). This shows a weak tidal choking.

The magnitude of choking can be assessed by tidal range ratio between inside and outside of the choked inlet (Glenne and Simensen, 1963; Hill, 1994; Rydberg and Wickbom, 1996). Since the dominance of M_2 tide in this sea area, tidal choking can be quantified using the M_2 amplitude difference between the location at 10 km (inside the East Entrance) and the location at 13 km (outside of the East Entrance). The two locations have the same depth of ~60 m before the project. Results are given in Table 5. Bigger M_2 amplitude drop and more delayed M_2 phase imply a stronger tidal choking.

Comparing Exps B3 and CR, the first dam decreases M_2 amplitude difference, but had no effect on its phase difference. The second dam hardly affects the tidal choking at the East Entrance. The clearly larger difference of M_2 amplitude and more delayed M2 phase in Exp B5 compared to Exp B4 show that the tidal choking at the East Entrance is significantly enhanced by the third dam, which is located very close to the East Entrance. Table 5 also shows that the third wharf further enhances the tidal choking. The deeper topography at the East Entrance can compensatorily decrease the tidal choking (compare Exps A4 and B4, Exps A8 and B8). This mechanism has been revealed by many simplified tidal choking models (for example, Van de Kreeke, 1988; Hill, 1994). However, the tidal choking in Exp A5 is stronger than that in Exp B5. This is due to the reclamation at the southern-island chain (Fig. 1b), especially at Dayangshan Island, which decreased the width of the East Entrance and led to the cross-sectional area of the East Entrance reduced by ~7%. In overall, the YDH project plays a dominant role in the enhancement of the tidal choking at the East Entrance, which is partly compensated by the souring in the channel.

Confined by momentum balance, the drop in water level leads to acceleration of flow through a choked inlet (Stigebrandt, 1980). The acceleration can be seen in the East Entrance (Fig. 7d). Before the project, the M_2 major-axis magnified nearly 0.3 m s^{-1} relative to that at ~13 km from the cross section when water passing through the East Entrance. The acceleration changed little by the first and second dams, but is enhanced ~0.1 m s^{-1} by the third dam, and strengthened further by the third wharf.

Previous studies indicated that two mechanisms can contribute to the tidal choking in a narrow channel: the jet induced water level drop forced by Bernoulli law and the friction induced energy loss (Keulegan, 1967; Stigebrandt, 1980). For a narrow long channel, bottom friction is the main reason for choking (Hill, 1994; MacMahan et al., 2014). While the momentum balance shows that the friction is not crucial in the choked East Entrance (Fig. 7f). During high velocities, the alongstream momentum balance is

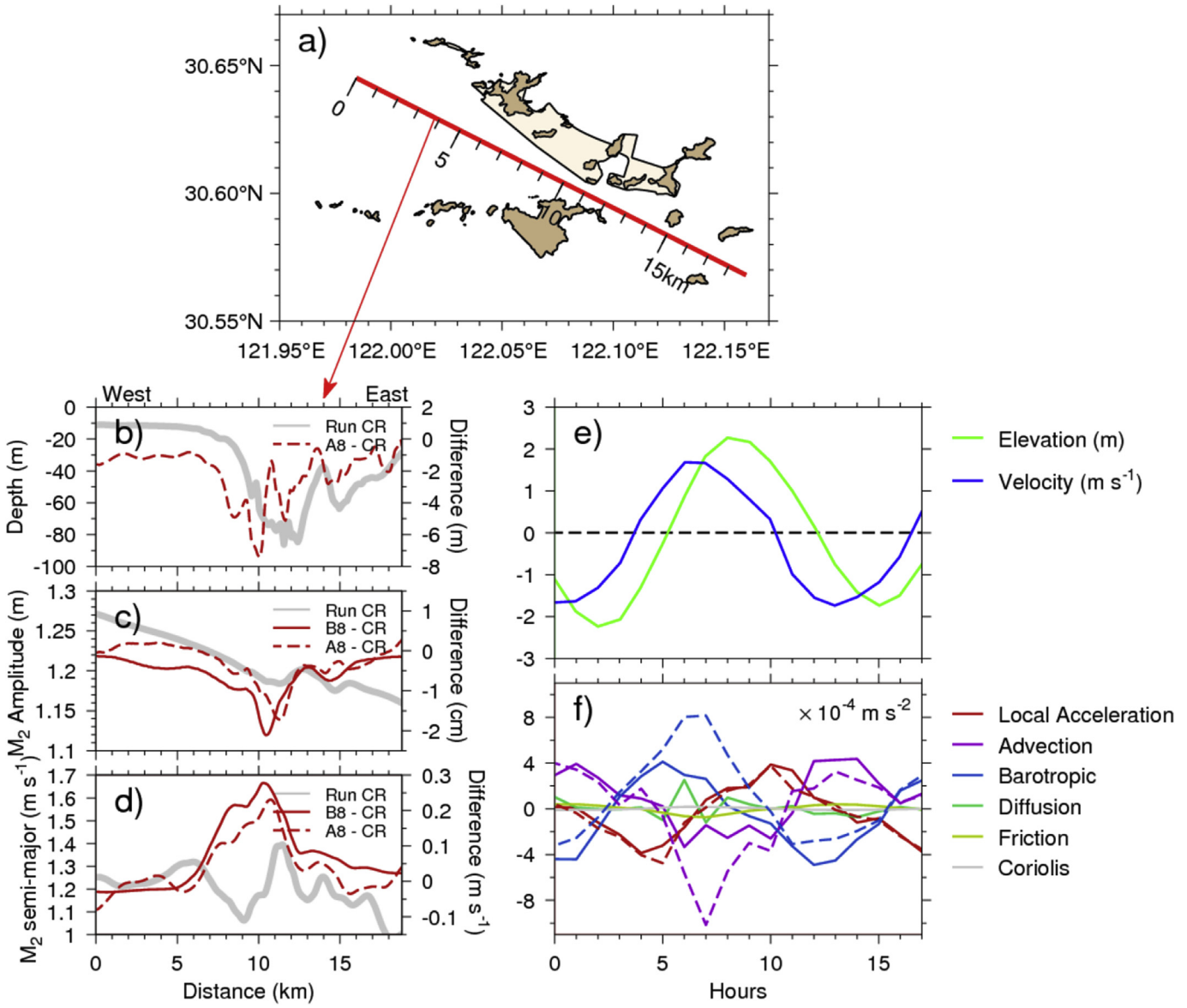

Fig. 7. (a) Location of the cross section for analysis of tidal choking in the East Entrance. The distances relative the west endpoint are labelled. (b), (c) and (d) show the results of depth, M_2 amplitude and the semi-major axis of M_2 current along the cross section shown in (a), respectively. Bold grey lines show the results in Exp. CR; the red solid and dashed lines show the results of Exp B8 − CR and Exp A8 − CR, respectively. (e) The elevation (green) and depth-averaged alongstream velocity (blue) in centre of the East Entrance. (f) The momentum balance (along the cross section shown in Fig. 7a) in centre of the East Entrance (averaged in the segment from 10.5 km to 12 km; solid lines: Exp CR; dash lines: Exp B8). (For interpretation of the references to colour in this figure legend, the reader is referred to the web version of this article.)

Table 5
The differences of M_2 amplitudes and phases between the location of 10 km and the location of 13 km at the cross-section displayed in Fig. 7.

Experiments	CR	A3	A4	A5	A8	B3	B4	B5	B8
Amplitude difference (cm)	−0.8	−0.3	−0.1	−2.2	−1.4	−0.3	−0.3	−0.9	−2.0
Phase difference (°)	3.1	3.0	2.8	3.8	3.3	3.1	3.0	3.4	3.6

dominated by horizontal advection and barotropic gradient, behaving a quasi-Bernoulli flow (Fig. 7e and f). Horizontal diffusion and bottom friction play a second role with magnitude one order smaller. While during slack water, the momentum balance is dominated by local acceleration and barotropic gradient, following linear wave dynamics. These results are coincident to observations at the short shallow Tauranga Harbour, New Zealand (Vennell, 2006) and the model results of Beaufort Inlet, North Carolina (Hench and Luettich, 2003). Thus, the Bernoulli law forced elevation drop is the substantial mechanism for the choking in the East Entrance.

The essence of the Bernoulli law is the transformation between tidal potential energy and tidal kinetic energy. The elevation drop means the energy transferred from tidal potential energy to tidal kinetic energy. Stronger choking, implying greater elevation drop, means more tidal potential energy is transferred to tidal kinetic

energy. This is confirmed by the energy budget in the East Entrance, where the percentage of potential energy decreases from 28.4% in Exp. CR to 26.1% in Exp. B8. The scouring in the channel weakens the tidal choking effect and results in a 26.7% of potential energy in Exp. A8.

As mentioned above, dams in the northern island chain decreased tidal amplitude in the lee, i.e., in the IHA. This can contribute to a stronger barotropic gradient pressure in the remaining channels. However, the third dam has induced tidal amplitude decrease in the sea area just adjacent to the East Entrance, thus forced stronger tidal choking in it. The tidal-amplitude-decrease area induced by the previous two dams are much further away from the East Entrance and thus result in little influence on the tidal choking in the East Entrance. For the third wharf, it has largely changed the geometry of the East Entrance (lengthened the East Entrance from 2 km to 4 km, narrowed it by ~ 5%), which can further increase the tidal choking effect as has been shown in the previous studies (Stigebrandt, 1980; Hill, 1994). But the scouring in the East Entrance would decrease the tidal choking effect.

5. Conclusions

When tide propagates through a long, narrow channel, its amplitude reduces and phase lag, which phenomena is called tidal choking. In this study, the changes of tidal choking in the Yangshan deepwater Harbour (YDH), Shanghai, China is studied, adopting a community ocean model FVCOM. The results show that the dams of channels can decrease tidal amplitude on their lee side directly, and simultaneously increase the tidal amplitude on the stoss side. Meanwhile, the dams decrease current on both sides of it, and it is found that near the dam, there are also two patches accompanying with current enhancement.

Stronger tidal choking effect is found in the East Entrance. The nine experiments based on the FVCOM model further reveal that this stronger choking is mainly due to the construction of the third dam and the third wharf. A qusi-Bernoulli flow is found in the choked channel during high velocities, showing the limited role of friction. The third dam decrease tidal amplitude adjacent to the East Entrance and thus increase the barotropic gradient pressure in the East Entrance, which can induce stronger jet in it and result in the stronger tidal choking effect. While the third wharf induces stronger tidal choking in the East Entrance via lengthening and narrowing it. This stronger choking effect is then compensatorily decreased by the scouring in the East Entrance.

The stronger tidal choking also results in larger tidal energy flux at the East Entrance, and the scouring on this channel further enlarges the tidal energy flux. Since the limited tidal energy flux in the northern-island chain, constructions on it bring only a little change to the total tidal energy density in the IHA, but obvious changes in the spatial distribution of tidal energy. In the IHA, the variations in tidal constants and other tidal characteristics have extreme spatial complexity, especially when the bathymetric changes are considered. The spatial complexity indicates that the increase in tidal constants around Station XYS is a local feature.

The Yangshan Harbour properly uses the jet of the East Entrance to maintain the depth in the navigation channels and harbour basins. In comparison with the Deep Navigation Channel of the North Passage of Shanghai Port, this project is a successful story from dredging point of view, which may provide management strategies for other harbours or navigation channels with strong sedimentation.

According to the numerical results of this study, it seems that a dynamic equilibrium exist in the tidal choking and the bathymetry of the choked channel, or morphology of the sea area. The interaction of them is a subject for our future study. Moreover, although these results are site-specific, the findings may be applicable to tidal dynamics in other island-building activities near the open sea, such as the dramatic reclamation of islands in the South China Sea.

Acknowledgments

The authors thank to the anonymous reviewers and the Editors for the constructive comments. We are also grateful to Mr. Rongshun Shao at the China Communications Construction Company Third Harbour Consultants Co., Ltd. for providing the observed data of bathymetries and water level used in this study. All the model settings and simulated results will be made available upon request to Prof. Pingxing Ding (Email: pxding@sklec.ecnu.edu.cn). The harmonic analysis of tides in this paper is performed using MATLAB T_Tide package, which is developed by Rich Pawlowicz, and available for download at http://www.eos.ubc.ca/~rich/t_tide/t_tide_v1.3beta.zip. The FVCOM source code for tidal simulation is downloaded from the SMAST website at http://fvcom.smast.umassd.edu/fvcom/. Wenyun Guo is awarded by the Fund of East China Normal University for Overseas Studies and the Fund of State Key Laboratory of Estuarine and Coastal Research for Overseas Studies. This work was supported by the Open Research Fund of State Key Laboratory of Estuarine and Coastal Research. (Grant number SKLEC-KF201608). Wenyun Guo and Pingxing Ding are supported by the National Natural Science Foundation of China (NSFC) (No. 41476076). Jianzhong Ge is funded by NSFC (No. 41306080). Dehai Song is supported by NSFC (No. 41406097) and General Financial Grant from the China Postdoctoral Science Foundation (No. 2014M550373). This is publication no. 25 of the Sino-Australian Research Centre for Coastal Management.

References

Allen, J.I., Somerfield, P.J., Gilbert, F.J., 2007. Quantifying uncertainty in high-resolution coupled hydrodynamic-ecosystem models. J. Mar. Syst. 64, 3–14. http://dx.doi.org/10.1016/j.jmarsys.2006.02.010.

Byun, D.S., Wang, X.H., Holloway, P.E., 2004. Tidal characteristic adjustment due to dyke and seawall construction in the Mokpo Coastal Zone, Korea. Estuar., Coast. Shelf Sci. 59, 185–196. http://dx.doi.org/10.1016/j.ecss.2003.08.007.

Chen, C., Beardsley, R.C., Cowles, G., 2006. An unstructured grid, finite-volume coastal ocean model (fvcom) system. Oceanography 19, 78–89.

Chen, C., Beardsley, R.C., Cowles, G., 2013. An Unstructured Grid, Finite-volume Coastal Ocean Model: FVCOM User Manual.

Chen, C., Gao, G., Qi, J., Proshutinsky, A., Beardsley, R.C., Kowalik, Z., Lin, H., Cowles, G., 2009. A new high-resolution unstructured grid finite volume Arctic Ocean model (AO-FVCOM): an application for tidal studies. J. Geophys. Res. 114.

Chen, S., 2000. Erosion and accretion characteristics and their causes in the Qiqu Archipelago in the recent century. Mar. Sci. Bull. 19 (1), 58–67 (In Chinese).

Fang, G., Kwok, Y., Yu, K., Zhu, Y., 1999. Numerical simulation of principal tidal constituents in the south China sea, Gulf of Tonkin and Gulf of Thailand. Cont. Shelf Res. 19, 845–869.

Foreman, M.G.G., Henry, R.F., Walters, R.A., Ballantyne, V.A., 1993. A finite element model for tides and resonance along the north coast of British columbia. J. Geophys. Res. 98, 2509–2531. http://dx.doi.org/10.1029/92JC02470.

Furukawa, K., Wolanski, E., 1998. Shallow-water frictional effects in island wakes. Estuar., Coast. Shelf Sci. 46, 599–607.

Ge, J., Ding, P., Chen, C., Hu, S., Fu, G., Wu, L., 2013. An integrated East China Sea–Changjiang Estuary model system with aim at resolving multi-scale regional–shelf–estuarine dynamics. Ocean. Dynam. 63, 881–900. http://dx.doi.org/10.1007/s10236-013-0631-3.

Glenne, B., Simensen, T., 1963. Tidal current choking in the landlocked fjord of NordÅsyatnet. Sarsia 11, 43–73. http://dx.doi.org/10.1080/00364827.1963.10410284.

Hench, J.L., Luettich, R.A., 2003. Transient tidal circulation and momentum balances at a shallow inlet. J. Phys. Oceanogr. 33, 913–932.

Hill, A.E., 1994. Fortnightly tides in a lagoon with variable choking. Estuar., Coast. Shelf Sci. 38, 423–434. http://dx.doi.org/10.1006/ecss.1994.1029.

Keulegan, G.H., 1967. Tidal Flow in Entrances; Water-level Fluctuations of Basins in Communication with Seas (DTIC Document).

Kjerfve, B., 1986. Comparative oceanography of coastal lagoons. In: Wolfe, D.A. (Ed.), Estuarine Variability. Academic Press, pp. 63–81. http://dx.doi.org/10.1016/B978-0-12-761890-6.50009-5.

Kjerfve, B., Knoppers, B.A., 1991. Tidal choking in a coastal lagoon. In: Parker, B. (Ed.), Tidal Hydrodynamics. John Wiley, pp. 169–181. http://dx.doi.org/10.1016/S0422-9894(08)70006-0.

Li, N., 2009. Study on Effects of Changes in Hydrodynamic and Sediment Conditions on the Seabed Erosion and Siltation by Yangshan Deepwater Port Projects in Qiqu Archipelagos. East China Normal University, Shanghai, China (In Chinese).

Li, L., Wang, X., Sidhu, H., Williams, D., 2011. Modelling of three dimensional tidal dynamics in Darwin Harbour, Australia. Anziam J. 52 (2010).

MacMahan, J., van de Kreeke, J., Reniers, A., Elgar, S., Raubenheimer, B., Thornton, E., Weltmer, M., Rynne, P., Brown, J., 2014. Fortnightly tides and subtidal motions in a choked inlet. Estuar. Coast. Shelf Sci. 150 (Part B), 325–331. http://dx.doi.org/10.1016/j.ecss.2014.03.025.

Moody, J.A., 1988. Small-scale inlets as tidal filters. In: Aubrey, D.G., Weishar, L. (Eds.), Hydrodynamics and Sediment Dynamics of Tidal Inlets. Springer, pp. 137–156. http://dx.doi.org/10.1029/LN029p0137.

National Ocean Service, 2000. In: Hicks, Steacy D. (Ed.), Tide and Current Glossary. Silver Spring, MD, Washington, p. 28.

Pawlowicz, R., Beardsley, B., Lentz, S., 2002. Classical tidal harmonic analysis including error estimates in MATLAB using T_TIDE. Comput. Geosci-Uk 28, 929–937. http://dx.doi.org/10.1016/S0098-3004(02)00013-4.

Ralston, D.K., Geyer, W.R., Lerczak, J.A., 2010. Structure, variability, and salt flux in a strongly forced salt wedge estuary. J. Geophys. Res. Oceans 115, C6005. http://dx.doi.org/10.1029/2009JC005806.

Rydberg, L., Wickbom, L., 1996. Tidal choking and bed friction in Negombo lagoon, Sri Lanka. Estuaries 19, 540–547. http://dx.doi.org/10.2307/1352516.

Song, D., Wang, X.H., Zhu, X., Bao, X., 2013. Modeling studies of the far-field effects of tidal flat reclamation on tidal dynamics in the East China Seas. Estuar., Coast. Shelf Sci. 133, 147–160.

State Key Laboratory of Estuarine and Coastal Research, East China Normal University (SKLEC, ECNU), China Communications Construction Company (CCCC) Third Harbour Consultants Co., Ltd, 2006. Analysis of Hydrodynamics and Sediment Environment and Change of Erosion and Deposition before and after the Construction of Yangshan Harbour (In Chinese).

Stigebrandt, A., 1980. Some aspects of tidal interaction with fjord constrictions. Estuar. Coast. Mar. Sci. 11, 151–166. http://dx.doi.org/10.1016/S0302-3524(80)80038-7.

Van de Kreeke, J., 1988. Hydrodynamics of tidal inlets. In: Aubrey, D.G., Weishar, L. (Eds.), Hydrodynamics and Sediment Dynamics of Tidal Inlets. Springer, New York, pp. 1–23.

Vennell, R., 2006. ADCP Measurements of Momentum Balance and Dynamic Topography in a Constricted Tidal Channel, vol. 36, pp. 177–188.

Wan, X.N., 2008. Response of the Strait-channel Effects to Harbour Project in the Yangshan Sea Area (Ph.D. thesis). East China Normal University, Shanghai, China (In Chinese).

Wang, Z.H., Li, L.Q., Chen, D.C., Xu, K.Q., Wei, T.Y., Gao, J.H., Zhao, Y.W., Chen, Z.Y., Masabate, W., 2007. Plume front and suspended sediment dispersal off the Yangtze (Changjiang) River mouth, China during non-flood season. Estuar. Coast Shelf S 71, 60–67. http://dx.doi.org/10.1016/j.ecss.2006.08.009.

Wolanski, E., Hamner, W.M., 1988. Topographically controlled fronts in the ocean and their biological influence. Science 241, 177–181.

Wu, H., Zhu, J., Shen, J., Wang, H., 2011. Tidal modulation on the Changjiang River plume in summer. J. Geophys. Res. Oceans 116, C8017. http://dx.doi.org/10.1029/2011jc007209.

Yang, Z., Cheng, H., Zhu, J., Li, S., 2012. Tidal dynamics of Yangshan harbor sea area and its response to the project. Acta Geogr. Sin. 9, 16 (In Chinese).

Ying, X.M., 2012. The Effect of Construction of Yangshan Deepwater Harbour on Morphological Change and Mechanism Analysis (Ph.D. thesis). East China Normal University, Shanghai, China (In Chinese).

Ying, X., Ding, P., Wang, Z.B., Van Maren, D.S., 2011. Morphological impact of the construction of an offshore Yangshan deepwater harbor in the Port of Shanghai, China. J. Coast. Res. 28, 163–173. http://dx.doi.org/10.2112/jcoastres-d-11-00046.1.

Yu, H., 2008. Study of Near-bottom Hydrodynamic and Sediment Character, Topography Evolution and Their Responses to the Construction of Yangshan Port in Qiqu Archipelago Sea Area (Ph.D. thesis). East China Normal University, Shanghai, China (In Chinese).

Yu, Z.Y., Li, S.D., Zhang, Z.L., 2013. Morphodynamical Response to the Construction of Yangshan Deepwater Harbour, Shanghai International Shipping Center. Science Press, Beijing (In Chinese).

Zu, T., Gan, J., Erofeeva, S.Y., 2008. Numerical study of the tide and tidal dynamics in the South China Sea. Deep Sea Res. 55, 137–154.